Kufa Journal of Engineering
Vol. 17, No. 1, January 2026, P.P. 204-230
Article history: Received 10 January 2025, last revised 14 March 2025, accepted 21 March 2025

NONLINEAR VIBRATION ANALYSIS OF ROTATING FUNCTIONALLY GRADED CNTS-REINFORCED COMPOSITE BEAMS: EFFECTS OF CNTS DISTRIBUTION PROFILES AND SYSTEM PARAMETERS

Al-hadrayi Ziadoon M. R.

Mechanical Engineering Department, Faculty of Engineering, University of Kufa, Najaf, Iraq, Email: zaidoonm.rahi@uokufa.edu.iq.

https://doi.org/10.30572/2018/KJE/170112

ABSTRACT

The nonlinear vibration behavior of rotating functionally graded carbon nanotube-reinforced composite (FG-CNTRC) beams is investigated with the impact of carbon nanotube (CNT) distribution patterns and system parameters. Five CNT distribution patterns are considered: Uniform Distribution (UD), Functionally Graded Λ-shaped (FG-Λ), V-shaped (FG-V), Outer (FG-O), and X-shaped (FG-X) to analyze their influence on the mechanical and dynamic properties of the beams. Utilizing Galerkin's method, the frequency ratios are determined with varying amplitudes, hub rotational radii, and volume fractions of CNTs. Statistical results reveal that the FG-Λ distribution gives the highest frequency ratio, enhancing by around 18-20% as compared to the UD configuration, while the FG-O and FG-X distributions represent intermediate improvements. The finding illustrates that a modification in the CNT volume fraction from 0.12 to 0.28 results in a significant increase in the system stiffness with increasing frequency ratios ranging from 1.36 to 2.0 at the peak amplitudes. Additionally, the effect of a hub radius (r = 0.5) also increases the frequency ratio by 6-8%, hence demonstrating the material and geometric parameters' synergy. These findings emphasize the importance of optimizing CNT distribution and system geometry for future engineering use, particularly in aerospace and energy systems.

KEYWORDS

Functionally Graded Carbon Nanotube-Reinforced Composite (FG-CNTRC), Rotating Beams, Nonlinear Vibration, CNT Distribution, Galerkin’s Method.

1. INTRODUCTION AND BACKGROUND

The study of advanced composite materials, such as carbon nanotube (CNT) reinforced composites, has been in great demand due to their exceptional electrical, thermal, and mechanical properties. These make them ideal substitutes for traditional laminated composites. The interest in the study stems from the challenge posed by delamination and micro-defects in composite materials, which compromise structural integrity and may result in potential failure. (Shen, 2009) considered the application of material gradation in nanocomposites, i.e., CNT-reinforced composite plates, and the advantage that functionally graded materials present regarding improved mechanical properties. (Bohlén and Bolton, 2013; Han and Elliott, 2007) demonstrated through molecular dynamics (MD) simulations that the Young's modulus in the direction of alignment is significantly increased for aligned composite beams by vertically aligned CNTs. Nevertheless, the classical mixture rule has been questioned regarding SWCNTs and a more refined mixture rule was established as described in (Griebel and Hamaekers, 2004). Also, the precise estimation of the effective wall thickness of SWCNTs has been taken into account in, hence establishing the groundwork for the mechanical behavior of CNT-reinforced composites (Wang and Zhang, 2008; Sadiq et al., 2025).

Rotating beam structures serve critical functions in aerospace, energy engineering, and transportation systems, e.g., spacecraft manipulators and propellers as (Chen et al., 2024) (Ranjbar and Feli, 2019). Such structures operate under extreme pressure and temperature conditions or free vibration by sandwich beam that was reinforcement honeycomb core, and this makes the structural reliability a top priority concern. CNT-reinforced composites are demonstrated to have extremely high strength and stiffness improvements over traditional carbon fiber-reinforced composites (Ziadoon, et al., 2023; Mohamed et al., 2022; Jasim and Abdulsamad, 2025). Additional studies have produced functionally graded carbon nanotube-reinforced composites (FG-CNTRCs), which are a novel class of materials with excellent potential for increasing the stiffness and reliability of rotating beam systems (Esen, Koç and Eroğlu, 2024; Al-Hadrayi et al., 2022; Al-hadrayi et al. , 2023 and ziadoon et al., 2022). The fabrication process tends to introduce geometric imperfections, which can influence structural performance as study explores both theoretically and experimentally the critical buckling load of combined columns (Xing-Wei et al., 2023). Vibration behavior of such structures is of significance to both design and operational performance.

The mechanical behavior of FG-CNTRC structures has been thoroughly investigated by previous studies. (Soni et al., 2022; Zhang et al., 2020) used plate models for analysis and comparison of the performance of uniform and functionally graded CNT distribution and

concluded that the functionally graded distribution optimizes structural performance. Buckling behavior of FG-CNTRC plates has been investigated and reported that the buckling load can be significantly increased by increasing the volume fraction of CNTs by a small amount. Vibration differential equation for rotating FG-CNTRC beams based on the Timoshenko beam theory in the presence of a uniform distributed temperature field and investigated the vibrational characteristics of functionally graded beams composed of ceramic and metallic constituents, wherein material properties vary along the length according to a power-law distribution. A finite element discretization approach was employed to incorporate this spatial material variation into the global mass and stiffness matrices. The primary objective was to determine the resulting natural frequencies and corresponding mode shapes (Mohammed Rahi , Z. and H. Khaleel , H. 2025, Khosravi, Arvin and Kiani, 2019 and Khaleel, Z.M.R. 2025). (Shenas, Malekzadeh and Ziaee, 2017) utilized Chebyshev-Ritz approach to examine pre-twisted rotating FG-CNTRC beams with focus on interplay among the pre-twist angle, rotatory motion, and CNT reinforcement on the natural frequency.

Geometrical imperfections, in the form of initial eccentricities and distortions, are unavoidable consequences of fabrication processes and significantly influence the static and dynamic response of structural members. (Kumar, 2018) used the Rayleigh-Ritz technique to investigate the free vibration response of hyperbolic flat shells with initial imperfections, while (Liu, Lv and Wu, 2019; Li, Tang and Hu, 2018; Ke, Yang and Kitipornchai, 2010 and Liu, Wu and Lyu, 2020) used a multi-scale approach to investigate the nonlinear fundamental resonance response of graphene microbeams with geometrical imperfections. These investigations determined that geometric imperfections decrease the nonlinear stiffness of the system and lower the hardening behavior of the frequency response curve. Nevertheless, the dynamic response of rotating FG-CNTRC beams with geometric imperfections is yet to be researched in particular with a focus on manufacturing-induced defects. The main focus of this study is to investigate the nonlinear free vibration performance of rotating FG-CNTRC beams in relation to CNT distribution pattern and system parameters. The key motivation of this study is to investigate the influence of the five distribution patterns (UD, FG-Λ, FG-V, FG-O, and FG-X) of CNTs on the mechanical and dynamic response of the beams. Additionally, the current study aims to study the effects of a variety of system parameters, such as angular velocity and hub radius, on dynamic response and frequency ratio of the beams. Through Galerkin's method together with the variational iteration approach, the study intends to check the effect of CNT volume fraction and distribution pattern on the system frequency response and stiffness. The results can be considered as required design parameters to develop FG-CNTRC beams in the engineering

profession, specifically in the aerospace and energy industries. In this work a dynamic model of rotating FG-CNTRC beams with rotational effects and geometric imperfections is developed. Through the addition of the scale effect and the efficiency parameters of CNTs, the modified rule of mixtures determines the equivalent material properties of the composite. The following analysis adopts Galerkin's approach: (1) discretization of applied equations of motion of the Euler-Bernoulli beam model and (2) the von Kármán geometric approximation of nonlinear effects. The developed nonlinear differential equations are treated by applying the variational iteration technique for frequency response and the stiffness properties of the system. Effects of CNT distribution patterns, volume fraction, hub radius, and angular velocity are systematically analyzed in numerical simulations. Compared to the literature and observations conclusions are drawn that help in determining the optimum design and performance of FG-CNTRC beams under rotating systems.

2. DYNAMIC MODELING OF ROTATING FG-CNTRC BEAMS

Exploring rotation effects during the nonlinear deterioration of functionally graded carbon nanotube-reinforced composite (FG-CNTRC) beams. This model provides a foundation for understanding the impacts of material properties, geometry, and dynamic features of FG CNTRC beams in nonlinear vibration. It is an effective method for creating novel composite beams with specific dynamic properties.

2.1. Material Properties and CNT Distribution Patterns

Functionally graded carbon nanotube-reinforced composite material is an innovative composite comprising an isotropic matrix and carbon nanotubes. Carbon nanotubes are uniformly aligned in a certain direction, resulting in gradient variations in the mechanical characteristics of the composite material along that axis. This study use carbon nanotubes to be uniformly dispersed across the thickness of the beam. Fig.1 illustrates five prevalent ways for distributing carbon nanotubes. The carbon nanoparticles align with these five distribution types. The volume ratio of the tube V_{cn} (z) may be articulated as the coordinate about the thickness direction of the beam. Functions designated as z expressed as following (Pang, Li, Du, et al., 2018):

$$\text{For UD:} \quad V_{cnt} = V_{tcnt} \tag{1}$$

$$\text{For FG-V: } V_{cnt} = (1 + \frac{2z}{h})V_{tcnt} \tag{2}$$

$$\text{For FG-}\Lambda\text{: } V_{cnt} = (1 - \frac{2z}{h})V_{tcnt} \tag{3}$$

$$\text{For FG-X: } V_{cnt} = 4\frac{|z|}{h}V_{tcnt} \tag{4}$$

$$\text{For FG-O: } V_{cnt} = 2 - 4\frac{|z|}{h}V_{tcnt} \tag{5}$$

Where h is the structure thickness, z is the coordinate value along the thickness direction, and V_{tcnt} is the total volume fraction of CNTs, which can be expressed as (Zhang et al., 2020):

$$V_{tcnt} = \frac{W_{cnt}}{W_{cnt}+\left(\frac{\rho_{cnt}}{\rho_m}\right)-\left(\frac{\rho_{cnt}}{\rho_m}\right)W_{cnt}} = 1 - V_m \quad (6)$$

In the Eq.6, Wcnt represents the mass fraction of CNTs, ρ_{cnt} and ρ_m represent their mass density, and Vm represents the entire volume fraction of the isotropic matrix.

The rotating FG-CNTRC beam with geometric defects is the subject of this section's investigation. Examine how variables affecting the system's frequency ratio λ affect the system, including hub radius, rotation speed, geometric flaws, carbon nanotube dispersion, and carbon nanotube volume percentage. Single-walled carbon nanotubes (SWCNT) are used as the reinforcement, while poly methyl methacrylate (PMMA) is chosen as the matrix. Table 1 illustrates the mechanical properties (Ke, Yang and Kitipornchai, 2010).

Table 1. Mechanical Properties (Ke, Yang and Kitipornchai, 2010).

Property, unit	Value
E_m, GPa	2.5
υ_m	0.3
ρ_m, Kg/m^3	1190
E_{cnt}, GPa	5.6
P_{cnt}, Kg/m^3	1190

Table 2 shows the performance parameters of carbon nanotubes at different volume fractions. Fig. 1 illustrates a schematic cross-section of the beam, illustrating the continuous distribution of carbon nanotubes in the direction of the beam's thickness.

Table 2. Carbon Nanotube Performance Parameters (Ke, Yang and Kitipornchai, 2010).

V_{tcnt}	0.12	0.12	0.12
η_1	0.137	0.137	0.137

Other parameters are set as: the length is 1 m, width is 0.04 m, height is 0.02 m, r = 0 to 0.6 , Ω^- is from 0 to 35, A_0 = 0.005, and the carbon nanotube distribution method is "O" shaped

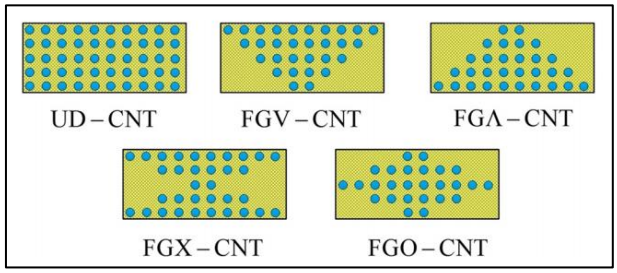

distribution.

Fig.1. Cross section of functionally graded carbon nanotube reinforced composites, including UD, FG-Λ, FG-V, FG-O, and FG-X (CNTRC) (Shi et al., 2017).

The equivalent material properties of a structure must be analyzed prior to examining its mechanical behavior. By introducing the scale effect and efficiency parameters of carbon nanotubes and utilizing the generalized mixing rate principle, the functionally graded carbon nanotube-enhanced composite depicted in Eq.7 and 8 can be produced, as per the modified

Mori-Tanaka model . The expressions of the equivalent material parameters (density ρ (z) and elastic modulus E (z)) as the following (Roy, Petrova and Mitra, 2018):

$$E(z) = \eta_1 V_{tcn}(z) E_{tcn} + V_m(z) E_m \quad (7)$$

$$\rho(z) = V_{tcn}(z)\,\rho_{tcn} + V_m(z)\,\rho_m \quad (8)$$

The elastic modulus of the matrix material and the carbon nanotube are denoted by Em and Ecn, respectively, in the formula. The performance parameter of the carbon nanotube, η_1, is determined through molecular dynamics. The matrix material and the carbon nanotube are represented by V_m (z) and V_{cn} (z). V_{cnt} (z) + V_m (z) = 1 is the volume fraction of the tube at any thickness of the beam. The degradation functions in the context of FG-CNTRC beams refer to the variation in material properties (e.g., stiffness and mass distribution) due to the non-uniform distribution of CNTs. The volume fraction of CNTs directly influences the effective elastic modulus and density of the composite, as described by the modified rule of mixtures Eqs.7 and 8.

2.2. Geometric Imperfections and Rotating Beam Model

Geometric imperfections include early bending as well as eccentricity and similar anomalies. This paper investigates mainly the geometrical faults of the first bending form. Fig. 2 illustrates the rotating FG-CNTRC beam and shows the first bending of a geometric model. This section defines the Cartesian coordinate system o - xyz with the coordinate origin at the midpoint of the beam's left end. The x-axis represents the length of the beam, the y-axis describes its width, and the z-axis extends along the beam's height direction. direction of thickness. The dimensions of the beam are denoted by L for length, b for breadth, and h for thickness. The beam is affixed to a hub of radius R and spins around a fixed axis in the xoy plane at a constant angular velocity Ω. W* denotes the displacement resulting from geometric imperfections.

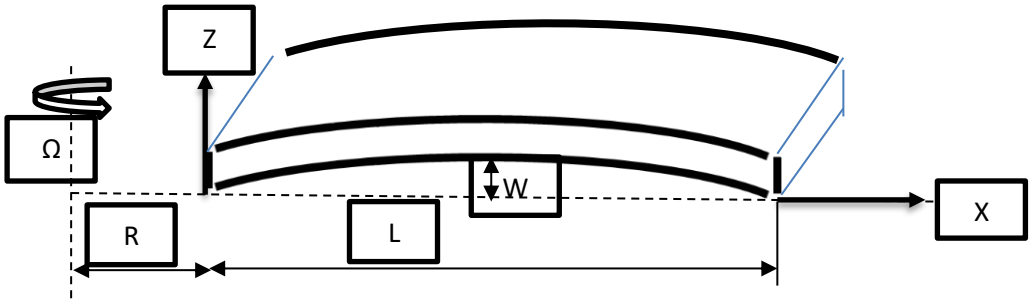

Fig.2. Geometric model of a rotating beam with geometric defects.

The displacement field at any point on the beam can be expressed by Eqs.9 to 11 in the Cartesian coordinate system, according to the Euler-Bernoulli beam theory (Pang, Li, Jing, et al., 2018; Li et al., 2019):

$$U1(x, y, z, t) = -zW' \quad (9)$$

$$U2(x, t) = 0 \quad (10)$$

$$U3(x,t) = W(x,t) + W^*(x) \quad (11)$$

According to the formula, W (x, t) is the transverse direction of the point on the neutral axis in the z and y directions, and Ui (i=1, 2, 3) is the displacement component of any point on the beam in the x, y, and z axis directions. displacement; the derivative of the function with respect to x is denoted by the symbol $(\cdot)'$.

The geometric defect displacement function, W* (x), is written as:

$$W^*(x) = A_o L \sin\left(\frac{\pi x}{L}\right) \quad (12)$$

The dimensionless amplitude of geometric flaws is denoted by A_o in the expression.

Eq.13 illustrates the strain-displacement relationship of the rotational FG-CNTRC beam with geometric flaws after introducing the von Kármán geometric nonlinear hypothesis:

$$\varepsilon_x = -zW'' + \frac{1}{2}(W')^2 + W'W'^* \quad (13)$$

The system's potential energy, or UP, may be written as follows:

$$U_P = \frac{1}{2}\int_0^L [EI(W'')^2 + \frac{1}{4}EA(W')^4 + \frac{1}{2}EA(W')^3W'^* + 12\,EAW'^*(W')^3 + EAW'(W'^*)^2]\,dx \quad (14)$$

The bending stiffness of the beam is denoted by EI, while the tensile stiffness is denoted by EA. These values can be expressed as Eqs 15 and 16 respectively:

$$EI = \iint E(z)y^2\,dA \quad (15)$$

$$EA = \iint E(z)\,dA \quad (16)$$

Eq.17 can be used to represent the kinetic energy T of the system:

$$T = \frac{1}{2}\int_0^L m\dot{W}^2 dx \quad (17)$$

The linear density of the beam is denoted by m in the Eq.18:

$$m = \iint \rho(z)\,dA \quad (18)$$

Eq.19 can be used to express the centrifugal force work W_C:

$$W_c = \frac{1}{2}\int_0^L \left[mR\Omega^2(L-x) + \frac{1}{2}m\Omega^2(L^2-x^2)(W')^2\right]dx \quad (19)$$

Hamilton's principle is employed because it provides a variational framework that is particularly well-suited for deriving the governing equations of motion for dynamic systems, including those with nonlinearities. Hamilton's principle, in contrast to other variational methods, involves kinetic, potential, and external work, making it suitable for studying the dynamic behavior of rotating beams. It also facilitates the systematic embedding of geometric nonlinearities and centrifugal impact that are vital to properly modelling FG-CNTRC beam vibration, (Reddy, 2007):

$$\boldsymbol{\delta\int_{t_1}^{t_2}(T - U_p + W_c)dt = 0} \quad (20)$$

In the equation, t_1 and t_2 denote temporal variables, whereas δ is the symbol for variation. Substitute Eqs.14,17, and 19 into Eq.20 to get the governing equation:

$$m\ddot{W} + EIW'' - m\Omega^2\left[R(L-x) + \frac{1}{2}(L^2 - x^2)\right]W'' + m\Omega^2(R+x)W' - EA(W'^{*})W'' -$$
$$2EAW'^{*}W''^{*}W' - 3EAW'^{*}W'W'' - \frac{3}{2}EA\left[W''^{*}(W')^2 + W''(W')^2\right] = 0 \qquad (21)$$

Eq.21 demonstrates that the linear component of the control equation will be altered by the presence of geometric defects, which will also result in the emergence of quadratic nonlinear terms in the control equation. The governing equation Eq. 21 describes the dynamic equilibrium of the rotating FG-CNTRC beam with geometric nonlinearities as well as effects of centrifugal stiffening and geometric imperfections. The nonlinear terms stem from the physical interpretation of the equation which states that it balances the inertial forces (mass acceleration), elastic restoring (bending and axial stiffness), and the centrifugal forces originating from rotation. The terms bend include bending stiffness, axial stiffness, and the effects of rotational motion. The von Karman strain displacement relation, which encompasses large deformation, gives rise to the nonlinear terms.

2.3. Dimensionless Formulation and Governing Equations

The following dimensionless parameters:

$$\zeta = \frac{x}{L}, w = \frac{W}{L}, \qquad w^* = \frac{W^*}{L}, r = \frac{R}{L}, c_1 = \frac{EI}{E_m I_y}, c_2 = \frac{m}{\rho_m bh}, c_3 = \frac{A_{11}}{E_m I_y},$$
$$\overline{\Omega^2} = \frac{\rho_m bhL^4\Omega^2}{E_m I_y}, \qquad \tau = t\sqrt{\frac{E_m I_y}{\rho_m bhL^4}} \qquad (22)$$

To obtain the dimensionless form of the governing equation, substitute Eq.22 into Eq.21:

$$c_2\ddot{w} + c_1 w'' - c_2\overline{\Omega^2}\left[r(1-\zeta) + \frac{1}{2}(1-\zeta^2)\right]w'' + c_2\overline{\Omega^2}(r+\zeta)w' - c_3(w'*)^2 w'' - 2c_3 w'*$$
$$w''*w' - \frac{3}{2}c_3[w''*w'^2 + 2w'^{*}w'w''] - \frac{3}{2}c_3\, w'^2 w'' = 0 \qquad (23)$$

Eq.23 is the dimensionless governing equation of the nonlinear vibration of functionally graded carbon nanotube-reinforced composite (FG-CNTRC) beams with rotation and geometric imperfections. The governing equation Eq. 21 is employed as a source equation to derive Eq.23 with the addition of dimensionless parameters Eq. 22 for easier analysis and to produce results that can be more generalized. Each of the terms in Eq.23 has a definite physical meaning that, when combined, describe the nonlinear vibration of rotating FG-CNTRC beams. The term$c_2\ddot{w}$ is the inertial force due to the transverse acceleration of the beam and represents its dynamic behavior in vibration. The term $c_1 w''$ is the bending stiffness, a measure of the beam's resistance to bending deformation due to bending moments. The term $c_2\overline{\Omega^2}\left[r(1-\zeta) + \frac{1}{2}(1-\zeta^2)\right]w''$

accounts for the centrifugal stiffening effect, which significantly increases the effective stiffness of the beam by rotation and is more significant at higher rotational speeds $c_2\overline{\Omega^2}(r+\zeta)w'$ represents the centrifugal force along the beam length, which generates axial tension and influences its vibration. The $c_3(w'^*)^2w''$ and $2c_3w'^*w''^*w'$, are a result of geometric nonlinearities from initial imperfections, and they reflect the interaction between initial curvature and bending deformation. Additionally, the terms $\frac{3}{2}c_3[w''^*w'^2+2w'^*w'w'']$ and $\frac{3}{2}c_3\,w'^2w''$ show nonlinear stiffness due to large deformations, the integrated coupling between bending and stretching under imperfections, and hardening of the frequency response of the beam at larger amplitudes. Together, these terms depict the total nonlinear dynamic behavior of the beam under rotational and geometric influences.

2.4. Nonlinear Free Vibration Analysis Using Variational Iteration Method

Given that the formula represents a nonlinear partial differential equation, this section first employs the Galerkin technique to discretize it into an ordinary differential equation, then expanding the displacement function w (ζ) as:

$$w(\zeta)=\sum_{i=1}^{n}\varphi_i(\zeta)q_i(\tau) \qquad (24)$$

Where n= 1,2,3….

These include the i-order trial function $\varphi_i(\xi)$ that satisfies the boundary conditions and the generalized coordinates of lateral displacement, $q_i(\tau)$.

Substitute Eq.24 into Eq.23 to derive the discretized equation. Then, multiply the corresponding trial functions of each order $\varphi_i(\xi)$ on both sides of the equation, integrate over the full length of the beam, and take the first order. Discretely obtain the following:

$$\ddot{q}+\gamma_1q+\gamma_2q^2+\gamma_3q^3=0 \qquad (25)$$

The discretized equation is obtained by substituting Eq.22 into Eq.21 Then, the corresponding trial functions of each order $\varphi_i(\xi)$ are multiplied on both sides of the equation, integrated across the whole length of the beam, and the first order, get:

$$\gamma_1=\frac{1}{X_1}\int_0^1[c_1\varphi_1''-c_2(r\overline{\Omega^2}\,(1-\zeta)+\frac{1}{2}\overline{\Omega^2}(1-\zeta^2))\varphi_1''-c_3w'*\varphi_1''-c_3w'*w''\varphi_1'+c_2\overline{\Omega^2}(r+\zeta)\varphi_1']\,\varphi_1dx \qquad (26)$$

$$\gamma_2=-\frac{3}{2X_1}c_3\int_0^1[w''^*(\varphi_1')^2+2w'*\varphi_1'\varphi_1'']\varphi_1dx \qquad (27)$$

$$\gamma_3=-\frac{3}{2X_1}c_3\int_0^1[(\varphi_1')^2]\varphi_1''\varphi_1dx \qquad (28)$$

$$X_1=c_2\int_0^1\varphi_1^2\,dx \qquad (29)$$

Where r is the hub radius dimensionless, which is the hub radius divided by the beam length.

$\varphi_i(\xi)$ is the Galerkin method trial functions used to approximate the displacement function $w(\zeta)$. The trial functions satisfy the boundary conditions of the beam. γ_1 is the linear stiffness coefficient in the discretized governing equation. γ_2 is the quadratic nonlinearity coefficient in the discretized governing equation. γ_3 is the cubic nonlinearity coefficient in the discretized governing equation. To get the frequency of this nonlinear system, first establish the starting value condition as follows:

$$q(0) = A \text{ and } \dot{q}(0) = 0 \quad (30)$$

In the equation, A denotes the starting amplitude. In order to resolve the ODE, the correction functional is as follows:

$$q_{n+1}(\tau) = q_n(\tau) + \int_0^{\tau} \Gamma(\tau)\{[q_n(\zeta)] + N[\overline{q_n}(\zeta)]\}\, d\zeta \quad (30)$$

In the formula, $q_n(\tau)$ denotes the n-th order approximate solution of Eq.25, $\Gamma(\tau)$ signifies the Laplace multiplier, and $\overline{q_n}(\zeta)$ represents the asymptotic variable component of $q_n(\tau)$, adhering to the condition: $\delta\overline{q_n}(\tau) = 0$. Furthermore, L [·] and N [·] refer to the linear and nonlinear operators of Eq.25, respectively, which can be articulated as:

$$L[q] = \ddot{q} + \omega_{n1}^2 q_1 \quad (31)$$

$$N[q] = \gamma_1 q + \gamma_2 q^2 + \gamma_3 q^3 - \omega_{n1}^2 q_1 \quad (32)$$

In the above equations, the frequency of the nonlinear system is ω_{n1}. The nonlinear frequency and frequency ratio of the system can be expressed with the equation:

$$\omega_{n1} = \sqrt{\frac{3A^2\gamma_3 + 4\gamma_1}{2}} \quad (33)$$

$$\lambda = \frac{\omega_{n1}}{\omega_L} \quad (34)$$

Where λ is the frequency ratio and ω_L is the linear natural frequency.

3. NUMERICAL RESULTS AND DISCUSSION

System interaction is primarily determined by the volume fraction of Carbon Nanotubes (CNTs) and its influence on Frequency Ratio (λ), with respect to Amplitude (A), at the dimension hub radius of 0 in all three Figs. 3-5. It also illustrates material properties, such as CNT distribution configuration, such as a zero-hub radius, which is in the case of either the minimum or non-existence of geometric rigidity. The system dynamic response is weaker in Fig. 3 (CNT volume fraction = 0.12), and λ peaks around 1.36, with an extrema of A (−0.008 and 0.008). A bit lower λ, indicating lower rigidity, and therefore less reinforcement at this lower volume fraction of CNT. It indicates that even without hub radius, a decreased concentration of CNT does not make up for the softness. Fig.4 shows in Fig.4 the system has a much firmer overall structure (CNT volume fraction = 0.17) compared to the first graph. The largest amplitudes have more clearly nonlinear curves with a maximum λ of approximately 1.6. The higher λ means that the stiffness of the system is markedly improved with increasing

concentration of CNT albeit with zero hub radius. For *A*=0, the symmetry value is constant since deformation is unaffected by any material distortion. The system reaction to this is quite stiffer in Fig.5 (CNT volume fraction = 0.28) but with amplitude that varies from −0.012 to 0.012 (or λ up to 2.0 at the extrema of A); this larger amplitude range and larger λ value, which compensated for the hub-radius absence, shows how much reinforcement the increasing CNT volume fraction provides to the system. As λ rise with the amplitudes corresponds to a strong overall nonlinear effect, the mechanical response of the system is strongly regulated by CNTs. However, when hub radius becomes zero, the only important variable of CNT remains the concentration fraction to contribute to the stiffness, frequency response among all members. Evolution from a gentle reaction emphasizes the importance of CNTs for both reinforcing the material and improving the dynamic stiffness at a lower CNT volume fraction (0.12) to a stiffer, more nonlinear response at a higher CNT volume fraction (0.28). The direct influence of CNTs on the system's behaviour is underscored by the absence of a hub radius, which renders them a dominant factor in the determination of the mechanical properties.

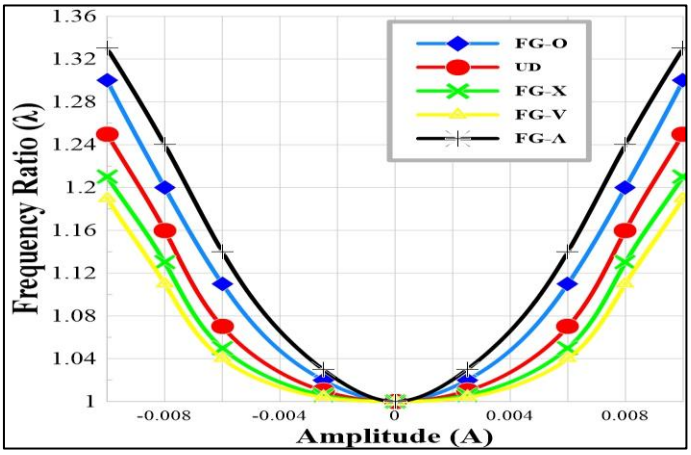

Fig. 3. The influence of the distribution pattern of carbon nanotubes on the frequency ratio (volume fraction =0.12 and r =0)

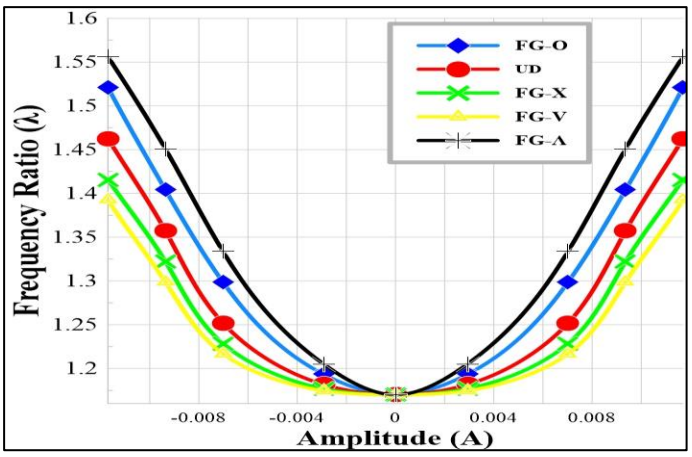

Fig. 4. The influence of the distribution pattern of carbon nanotubes on the frequency ratio (volume fraction =0.17 and r =0)

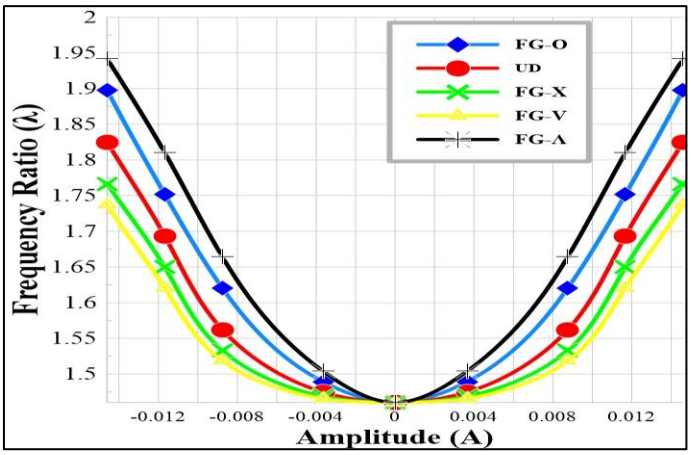

Fig. 5. The influence of the distribution pattern of carbon nanotubes on the frequency ratio (volume fraction =0.28 and r =0)

Figs. 6–8 illustrate how the dynamic response of the system is basically determined by the percentage of volume of Carbon Nanotubes (CNTs) and how this affects the Frequency Ratio (λ) vis a vis Amplitude (A). Instead of the zero-hub radius configuration, it becomes a hub radius of 0.25. This adds to the geometric stiffness of the system. Mechanical response of the system is determined by the geometric factor as well as the material attributes influenced by the CNT dispersion. In a narrower pattern, in Fig. 6, the dynamic response is comparatively shallow when λ is relatively close to 1.36 between extremes of A (-0.008 and 0.008). The low value of the increase in λ in respect of all zero-hub scenarios indicates that the larger radius in the hub compensates for the stiffness decrease that results from a smaller % CNT volume. Conversely, with very modest reinforcement of the CNTs, we see that a very less clear non-linear response has been given by L2V for the slightly slower curvature of the λ vs A graph. The system had better stiffness, in Fig. 7, where λ has a span of ~1.6 at the extremes of A, showing the system to be more rigid, which corresponds to the increased CNT content. The embedding of the hub radius results in a sharper curvature of the λ vs A plot, as well as a more noticeable nonlinearity at the higher amplitudes when the rigidity increases. The close symmetry of A=0 maintains the equilibrium of a response to deformation. In Fig. 8 (CNT volume percent = 0.28), we observe the most rigidity of the system, with λ reaching as high as 2.0 for the system and amplitude ranging between -0.012 and 0.012. The higher CNT volume percentage and geometric stiffness because of hub radius have markedly enhanced material properties. Dynamic rigidity was greatly improved by CNT, because of the significant nonlinearity and rapid increase in λ at larger amplitudes. With a wider amplitude range and a higher value of λ, it is considered a robust material, resistant to large deformations, without significantly softening. The increment in the CNT volume percentage from 0.12 to 0.28 is an effect of λ increasing and amplitude band widening. This implies that CNTs play an essential role in reinforcing the composites providing

higher stability and frequency responsiveness, while at hub radius (0.25) an entirely new dimension of stiffness is introduced--as can be seen in the higher λ values to zero hub structure. This geometric property enhances the CNT strengthening to be stronger and less linear in response. With an increase of the volume percentage of CNT, the λ versus A connection appears to be nonlinear. According to this behaviour, for CNT reinforcement to increase geometric stiffness in a combination, the material will be stronger to resist deformation. The dynamic reaction is ascribed to material-geometrical coupling. Carbon nanotubes act as nanoscale reinforcement, increasing stiffness and damping capacity of the composite fabric. The radius of hub affects the system through enhanced structural stability which occurs with great amplitude. The stiffness and frequency response of the system is determined by its volume fraction of CNT ratio and hub radius. This shift from a more flexible response at lower CNT fractions to a stiff nonlinear response at higher CNT fractions demonstrates that when modifying dynamic features in the system, such features matter.

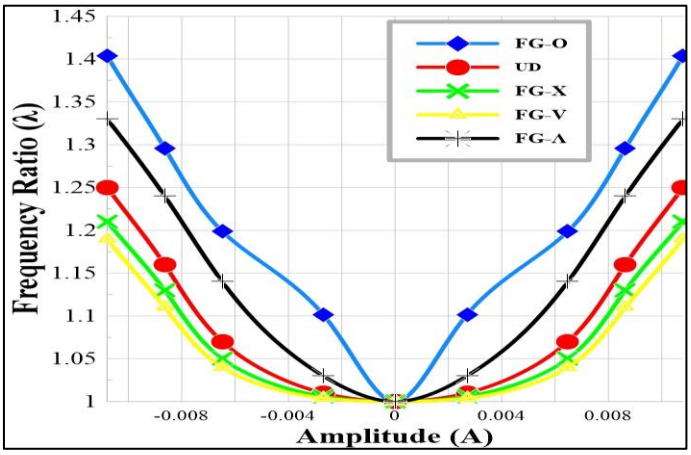

Fig. 6. The influence of the distribution pattern of carbon nanotubes on the frequency ratio (volume fraction =0.12 and r =0.25)

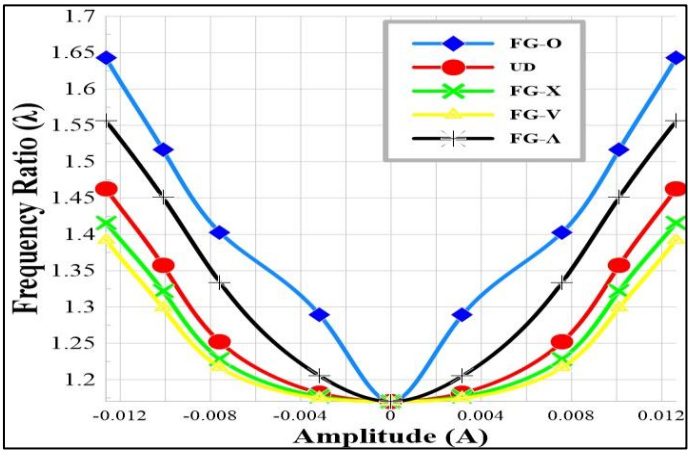

Fig. 7. The influence of the distribution pattern of carbon nanotubes on the frequency ratio (volume fraction =0.17 and r =0.25)

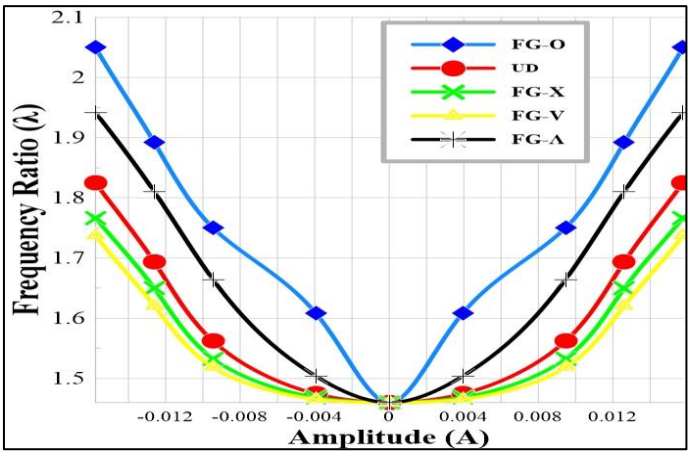

Fig. 8. The influence of the distribution pattern of carbon nanotubes on the frequency ratio (volume fraction =0.28 and r =0.25)

Therefore, the proportion of CNT volume and hub radius influence mechanically the behavior of a system. As CNT concentrations and hub radius increase, stiffer, more nonlinear responses are generated, where λ values are higher with magnitudes (see Figs. 9–11). Hub radius of the resulting design is equal to 0.5 compared to zero and 0.25 hub radii thus imparting increased geometric stiffness to the design. The mechanical response of the system is controlled by the geometric and also by the material property modulated between CNT distributions. Carbon nanotubes have been employed as nanoscale strengthening materials that exhibit the stiffness and damping properties of the material. This results to the large tensile and nonlinearities with higher λ-A ratios with the increased concentration of CNT. Moreover, the hub radius adds geometric rigidity, along with the properties of CNTs. The effects are to increase the λ values in Figs.6–8 relative to Figs.3–5. For low CNT volume fractions (0.12) the system has some resistance but low reinforcing strength. With more CNT volume fractionation (0.17, 0.28), this system shows an even stiffer and nonlinear behaviour but this has shown more importance of CNTs to improve dynamic stiffness. Such CNT distributions in these designs influence the rigidity and frequency response of the system. Overall, FG-Λ and FG-O generally lead to higher λ values, attributable to the better CNT placement, whereas UD (Uniform Distribution) exhibits lower λ due to its disadvantageous reinforcing state. Based on the CNT distributions, it was observed from all three CNTs, Functionally Graded Outer (FG-O) and Functionally Graded X-shaped (FG-X) presents the best performance with respect to Uniform distribution (UD). The FG-O structure is known for having greater CNT content at the outer surface which contributes to the material stiffness at high magnitude because of the stronger reinforcing of the main stress. Selective CNT dispersion with this FG-X structure yields an even stiffness and damping capability, especially in the middle ranges. Despite the moderate performance of the FG-Λ and FG-V shapes for an individualized CNT gradients configuration, no high λ indicates higher

values of the FG-O and FG-X configuration. In the simplified uniform distribution (UD), the worst amount of reinforcement is achieved, because it fails to avoid distortion due to the fact that it is not shaped with CNTs to obtain greater optimization in CNT localization. It indicates that the stiffness dynamics (Frequency response) are also influenced by the geometry of the CNTs inside the composite material, as the concentration percentage of CNTs does not only affect the dynamics of stiffness and frequency response. Through optimized CNT distributions (FG-O, FG-X) and additional geometrical reinforcement (hub radius) these systems have achieved improved mechanical properties, such as high λ values, and high nonlinearity and larger maximum amplitude range. These findings highlight the critical importance of dual physical-mechanical geometry properties together for the consideration of such design for structural systems for improved mechanical performance. This increase from flexible response at low CNT fractions to a much more nonlinear, rigid response at high fractions of CNT emphasizes that material reinforcement and geometrical design of CNT must adjust toward different dynamics required for the design phase.

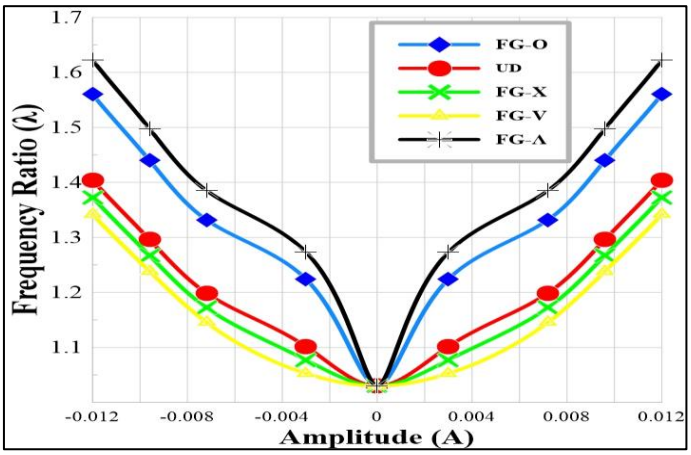

Fig.9. The influence of the distribution pattern of carbon nanotubes on the frequency ratio (volume fraction =0.12 and r =0.5)

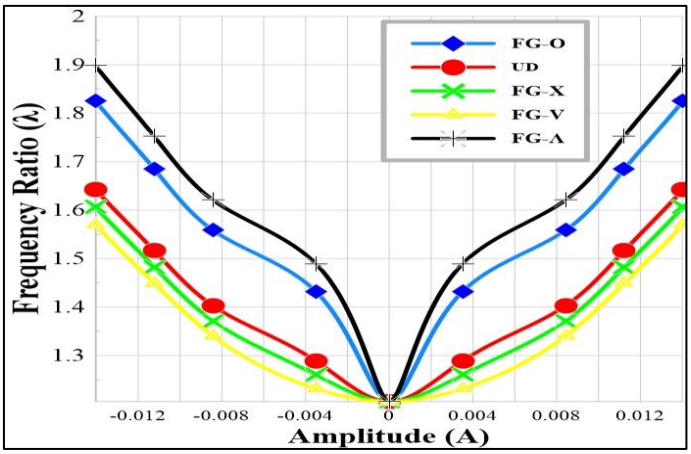

Fig.10. The influence of the distribution pattern of carbon nanotubes on the frequency ratio (volume fraction =0.17 and r =0.5)

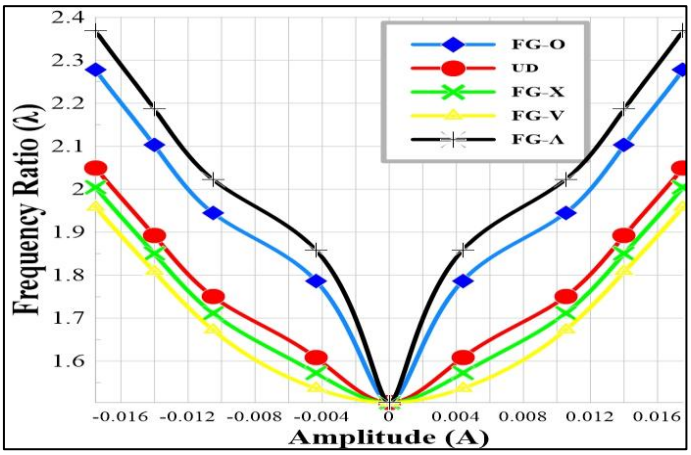

Fig.11. The influence of the distribution pattern of carbon nanotubes on the frequency ratio (volume fraction =0.28 and r =0.5)

The analysis concentrated on the impact of the volume fraction of Carbon Nanotubes (CNTs) (0.12, 0.17, 0.28) and r (0, 0.25, 0.5) on the linear natural frequency (ω_L) for various configurations (FG-O, FG-Λ, FG-X, FG-V, and UD) as a function of the dimensionless rotational speed ($\overline{\Omega}$) as illustrated in the Figs. 12-20.

At a CNT volume fraction of 0.12, as seen in Fig.12, the natural frequency (ω_L) is reduced across all configurations in comparison to higher volume fractions. At $\overline{\Omega}$=25, the FG-Λ configuration attains a peak frequency of roughly 76 rad/s, whereas the UD configuration maintains a lower frequency of about 68 rad/s. The FG-O, FG-V, and FG-X designs exhibit intermediate frequencies between 69 and 72 rad/s. The diminished natural frequencies in this instance may be ascribed to the decreased reinforcement afforded by the lesser quantity of CNTs, leading to reduced stiffness efficacy. The FG-Λ arrangement exhibits the most pronounced increase in (ω_L), signifying an exceptional material gradient distribution and enhanced resistance to deformation at elevated rotational speeds.

As the CNT volume percentage rises to 0.17, all configurations, as seen in Fig.13, have elevated values relative to the 0.12 scenario. At $\overline{\Omega}$ = 25, the FG-Λ configuration attains roughly 84 rad/s, while the UD configuration escalates to about 76 rad/s. FG-O and FG-V attain frequencies of around 78 rad/s, although FG-X is nearer to 77 rad/s. The increased CNT volume fraction enhances the total material stiffness, resulting in improved dynamic performance. The distinctions among the configurations become more apparent, with FG-Λ retaining its superiority owing to its optimized gradient distribution. The isotropic UD setup, despite improvements, remains inferior, highlighting the need of material customization.

At the maximum CNT volume fraction of 0.28, as seen in Fig.14, the natural frequency attains its zenith for all configurations. The FG-Λ configuration attains a value of around 100 rad/s at $\overline{\Omega}$=25, whereas the UD configuration reaches about 90 rad/s. FG-O, FG-V, and FG-X exhibit

frequencies of 93, 91, and 92 rad/s, respectively. The substantial CNT reinforcement significantly enhances stiffness, allowing the structure to withstand deformation more efficiently. The FG-Λ configuration's exceptional performance highlights its ideal material gradation, which strategically improves stiffness throughout the structure. Conversely, the UD design, albeit demonstrating improvement, remains the least efficient because to its isotropic material distribution, which fails to leverage the CNT reinforcement.

Throughout all volume fractions, the FG-Λ configuration consistently demonstrates the greatest (ω_L), with enhancements of roughly 10–12% compared to the next best configuration (FG-O) and around 18–20% relative to the isotropic UD design.

These trends arise due to the effect that the CNT volume fraction has on the configuration's gradient distribution and hence on the performance parameters. Increased CNT volume fraction acts as additional reinforcement, and due to its larger volume fraction, it also increases the stiffness and hence the natural frequency. This effect is even greater on functionally graded CNT (FG-Λ, FG-O, FG-X, FG-V) configurations with the CNT concentration being applied throughout the structure to achieve maximum stiffness and maximum deformation resistance. The FG-Λ is the state-of-the-art layout, which also has the best gradients among the configurations, indicating the advantages of carefully considered materials. The isotropic distribution of the UD configuration, on the other hand, does not benefit from the CNT reinforcement; it constantly produces consistently lower natural frequencies. The volume fraction of the CNT and material distribution dictate the natural frequency of the system. This property is improved by the gradients for FG-Λ and FG-O and stiffness increases with increasing concentration of CNT. These disparities are further exacerbated by the rotational speed, with FG-Λ exhibiting the most optimal performance in all circumstances.

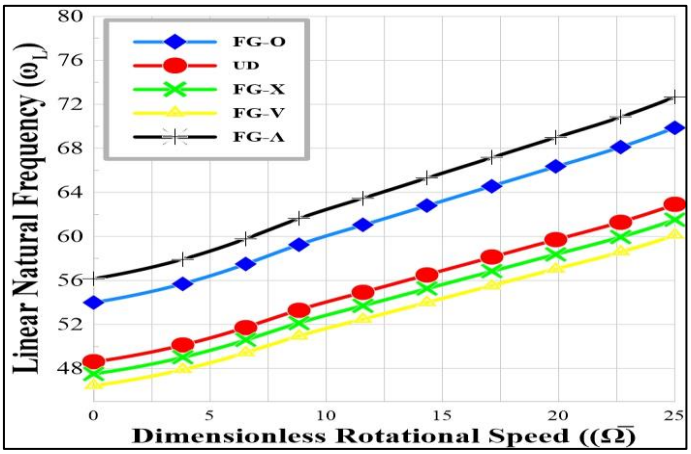

Fig.12. Variation of Linear Natural Frequency with Dimensionless Rotational Speed for CNT Volume Fraction0.12 and Material Configurations at Dimensionless Hub Radius r=0

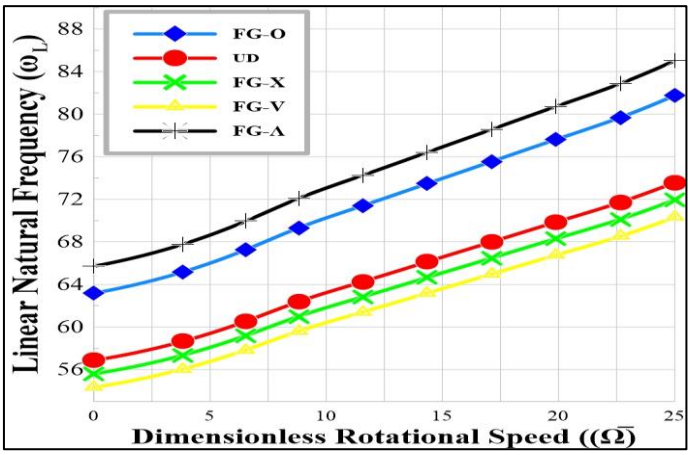

Fig.13. Variation of Linear Natural Frequency with Dimensionless Rotational Speed for CNT Volume Fraction 0.17 and Material Configurations at Dimensionless Hub Radius r=0

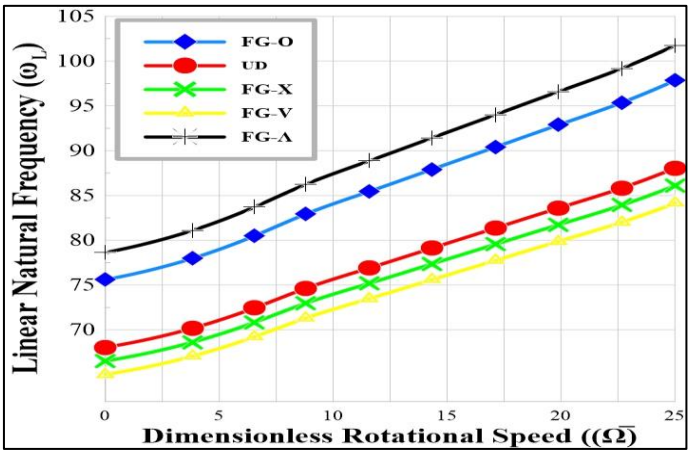

Fig.14. Variation of Linear Natural Frequency with Dimensionless Rotational Speed for CNT Volume Fraction 0.28 and Material Configurations at Dimensionless Hub Radius r=0.

Figs.15-17 present of the configurations at r=0.25 with previous results from r=0, with a particular emphasis on the impact of Carbon Nanotube (CNT) volume fractions (0.12, 0.17, and 0.28) on the linear natural frequency in relation to the dimensionless rotational speed. Consistent enhancements in stiffness and natural frequencies are seen across all configurations, with significant variations in the performance of gradient distributions.

For this CNT volume percentage of 0.12, the natural frequencies at r=0.25 are slightly higher than those at r=0. This is because the hub being expanded has the desired radius to reinforce the hub by effective use of materials. FG-V and UD have slightly lower values, around 70 rad/s and 69 rad/s, respectively. It results in weaker reinforcement at lower CNT content, but the stiffness of the hub increases to a sufficient extent to increase natural frequency. Since the configuration is optimized material gradient, the frequency increased universally by around 2–3%, so the FG-Λ configuration is better than r=0. Although isotropic, the UD design shares some advantages like hub radius, but it is the least efficient form.

With an increase in the CNT volume percentage to 0.17, the influence of the hub radius at

r=0.25 becomes more pronounced, augmenting the total stiffness of all designs. At Ω=25, the FG-Λ design reaches a peak frequency of roughly 88 rad/s, while the FG-O and FG-X configurations achieve frequencies between 84 and 85 rad/s. FG-V lags somewhat at 82 rad/s, while the UD configuration attains 80 rad/s. All configurations provide a uniform frequency increase of 4-5% relative to r=0. The FG-Λ design is the most efficient, leveraging the synergistic advantages of enhanced CNT content and the optimization of gradient dispersion. The UD configuration exhibits minor enhancements however remains deficient owing to its absence of customized material allocation.

At the maximum CNT volume fraction of 0.28, the natural frequencies at r=0.25 attain their apex levels across all configurations. The FG-Λ configuration attains around 104 rad/s at Ω=25, followed by FG-O and FG-X with frequencies ranging from 99 to 101 rad/s. The FG-V and UD designs provide somewhat reduced values, around 97 rad/s and 95 rad/s, respectively. Raising r to 0.25 further enhances stiffness, yielding an estimated frequency increase of 6-8% relative to r=0. The FG-Λ design persists in its superiority due to its capacity to strategically allocate CNTs across the structure, hence augmenting stiffness and resistance to deformation. The UD arrangement, while enhanced, continues to be less effective owing to its homogeneous material distribution. The noted increases in natural frequency from r=0.25 illustrate the substantial impact of hub radius on structural stiffness and dynamic performance. The improved material distribution offered by the FG designs (particularly FG-Λ and FG-O) guarantees appropriate reinforcement, resulting in significant enhancements in natural frequency. The FG-Λ design regularly surpasses others across all CNT volume fractions, exhibiting enhancements of 2-8% relative to r=0.

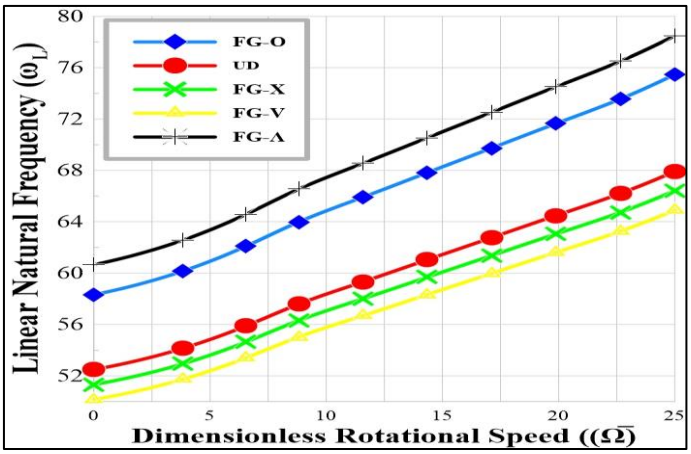

Fig. 15. Variation of Linear Natural Frequency with Dimensionless Rotational Speed for CNT Volume Fraction 0.12 and Material Configurations at Dimensionless Hub Radius r=0.25.

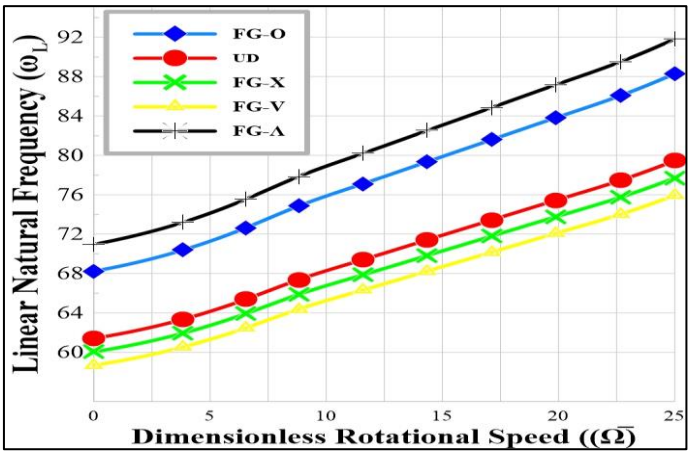

Fig.16. Variation of Linear Natural Frequency with Dimensionless Rotational Speed for CNT Volume Fraction 0.17 and Material Configurations at Dimensionless Hub Radius r=0.25.

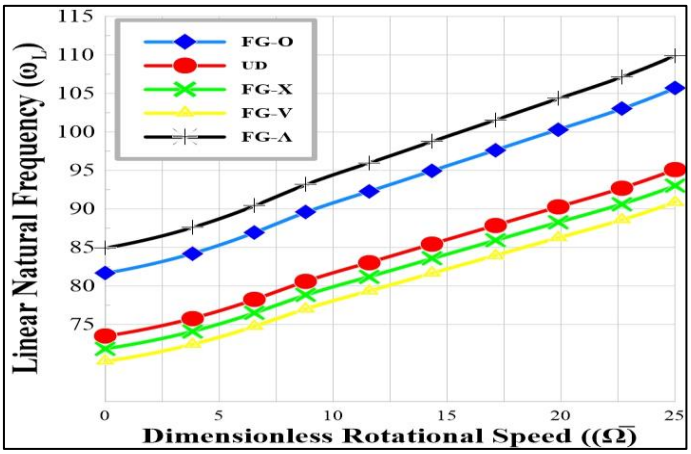

Fig. 17. Variation of Linear Natural Frequency with Dimensionless Rotational Speed for CNT Volume Fraction 0.28 and Material Configurations at Dimensionless Hub Radius r=0.25.

Figs 18-20 present of the configurations at r=0.5 with previous results from r=0, For all configurations at r=0.5, the natural frequencies are higher than those observed at r=0 when the CNT volume fraction is 0.12. The FG-Λ configuration maintains its highest frequency at Ω=25, with a value of approximately 83 rad/s, as opposed to 76 rad/s at r=0. The geometric factor, which increases the structure's rigidity, is responsible for the increase in natural frequency at r=0.5. Additionally, configurations such as FG-O and FG-V exhibit enhanced performance, despite the fact that their relative positioning remains consistent, with frequencies ranging from 75 to 78 rad/s. The isotropic UD configuration is behind, with a frequency of approximately 72 rad/s. This emphasizes the interaction between the hub radius and the CNT reinforcement in order to improve rigidity.

For CNT, at a volume fraction of 0.17, and with r=0.5, the overall natural frequencies become enhanced. With Ω=25, the apogee for the FG-Λ configuration is roughly 92 rad/s, well above the r=0 value of 84 rad/s. In all configurations, the larger hub radius is essential in terms of dynamic performances. The performance of FG-O and FG-V both exhibits similar level of

performance, and frequency near 86–88 rad/s, and FG-X slightly below 85 rad/s. Even with these improvements in the UD configuration, the poorest performance of UD appears to be approximately 80 rad/s, signifying the constraints of isotropic reinforcement on enhanced performance under rotational loading. The effect of r=0.5 occurs at the greatest CNT volume fraction maximum of 0.28. The maximum frequency of the FG-Λ is approximately 110 rad/s at Ω=25 compared to 100 rad/s at r=0, confirming that the increased stiffness of the FG-O, FG-V, and FG-X formations is manifested in the frequency at the region of 102–106 rad/s. While UD geometry was far from optimum (lowest frequency: 95 rad/s), the benefits of functionalized gradients are additionally evident by high CNT volume fraction, in particular the FG-Λ as the best material gradation. The performance of isotropic UD is still below the expected standard, making material customization crucial in deploying CNT reinforcement. Using the results for r=0 and r=0.5, the analysis suggests that, with increasing hub radius, the natural frequency is increased per configuration and CNT volume fractions as well. This effect can also be attributed to geometric stiffening with a larger hub radius which provides greater overall resistance to deformations during rotational loading. All values of r associated with larger CNT volume fractions demonstrate an increase of natural frequencies indicating that the material presents stiffness that exceeds the limited value on CNT volume fractions. An analogous finding is also observed for all the configurations, in which there is a remarkable enhancement of FG-Λ result from its excellent gradient distribution. FG-Λ is still better than all the other configurations – it is next for other configurations (FG-O, FG-V, and FG-X). As a result of the isotropic distribution of the materials, the UD configuration has the least advantage of being able to incorporate the potential of CNT reinforcement.

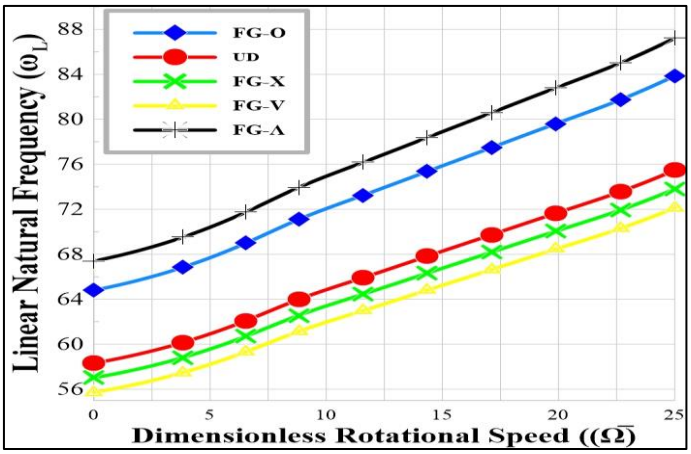

Fig.18. Variation of Linear Natural Frequency with Dimensionless Rotational Speed for CNT Volume Fraction 0.12 and Material Configurations at Dimensionless Hub Radius r=0.5.

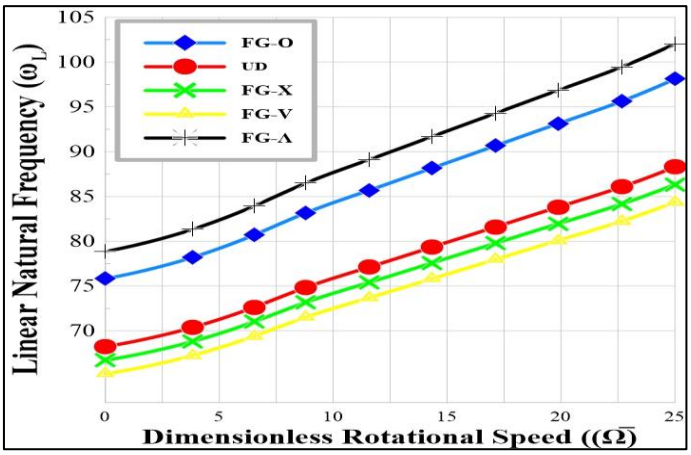

Fig. 19. Variation of Linear Natural Frequency with Dimensionless Rotational Speed for CNT Volume Fraction 0.17 and Material Configurations at Dimensionless Hub Radius r=0.5.

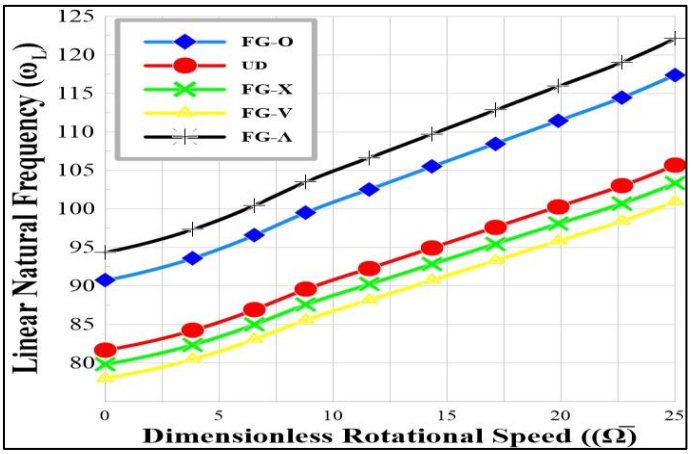

Fig. 20. Variation of Linear Natural Frequency with Dimensionless Rotational Speed for CNT Volume Fraction 0.28 and Material Configurations at Dimensionless Hub Radius r=0.5.

The natural frequency of the system increases considerably as the carbon nanotube volume fraction increases as shown in Table 3. This is due to the fact that the density of the composite material decreases, while the equivalent elastic modulus increases as a result of the incorporation of carbon nanotubes. This results in an increase in fundamental frequency and a commensurate increase in structural stiffness.

Table 3. Effect of FG-CNTRCs on fundamental frequency

Volume Fraction	UD	FG-Λ	FG-V	FG-O	FG-X
0.12	74.5	88.1	55.9	82.4	72.1
0.17	80.46	95.4	56.4	90.7	81.7
0.28	99.7	113.3	81.1	107.6	97.3

4. CONCLUSIONS

The Galerkin approach is employed to investigate the nonlinear frequency of the rotating FG-CNTRC beam with geometric imperfections in this work. The system's fundamental frequency and frequency ratio are investigated according to material properties, rotation impact, geometric imperfections, and other parameters. the main findings are as follows:

1. The pattern of distribution and volume fraction of carbon nanotubes (CNTs) significantly affects the fundamental frequency and frequency ratio of FG-CNTRC beams. The FG-Λ distribution always yields the maximum ratio of frequency, with an improvement of 18-20% over the UD case. Increasing the volume fraction of the CNTs from 0.12 to 0.28, the system stiffness is increased, with frequency ratios ranging from 1.36 to 2.0 for peak amplitudes.
2. Rotary motion and hub radius contribute to the linear stiffness of the structure, with 0.5 hub radius increasing the frequency ratio by 6-8%. The geometric stiffening effect and CNT reinforcement significantly enhance the dynamic behaviour of the beams.
3. Geometric imperfections introduce quadratic nonlinear terms in the governing equation, which causes a slight alteration of the linear frequency of the system. However, the nonlinear frequency is largely unaffected by such imperfections, which implies that the frequency ratio of the system is barely affected by geometric defects.
4. The study confirms that CNT distribution and system geometry optimization can greatly improve the mechanical and dynamic properties of FG-CNTRC beams. These findings are particularly relevant in the fields of aerospace and energy systems, where the role of high-performance materials is critical.

In general, dynamic analysis was particularly difficult in a real application to cover the material properties and CNT distribution of rotating FG-CNTRC beams, as manufacturing malformations (e.g., due to misalignment or voids) and deviations of their results from theoretical estimates are challenging. Nonlinear vibrations and geometric imperfections can induce expensive analysis costs and lead to uncertainties due to their computational load. If the CNT distribution and dynamic response are not well-defined for rotational measurements, it is also hard to obtain experimental verification. Such geometric imperfections like initial curvature attenuate the nonlinear stiffness and the frequency response can also alter, potentially compromising the structural integrity. As such, such effects need to be considered and explored for the effective realization of robust FG-CNTRC beam designs for high-performance engineering applications in aerospace and energy systems.

5. REFERENCES

Al-hadrayi, Z. M. R., Al-Khazraji, A. N. and Shandookh, A. A. (2023) ‘Mathematical Model of Properties and Experimental Fatigue Investigation at Elevated Temperatures of Functionally Gradient Materials’, Engineering and Technology Journal, 41, p. 7. http://doi.org/10.30684/etj.2023.137509.1352

Al-Hadrayi, Z. M. R., Al-Khazraji, A. N. and Shandookh, A. A. (2022) 'Investigation of Fatigue Behavior for Al/Zn Functionally Graded Material', Materials Science Forum, 1079, pp. 49–56. Available at: https://www.scientific.net/MSF.1079.49. https://doi.org/10.4028/p-8umjsp

Bohlén, M. and Bolton, K. (2013) 'Molecular dynamics studies of the influence of single wall carbon nanotubes on the mechanical properties of Poly (vinylidene fluoride)', Computational Materials Science, 68, pp. 73–80. https://doi.org/10.1016/j.commatsci.2012.10.010

Chen, C. et al. (2024) 'Free vibration exploration of axially functionally graded carbon nanotube-reinforced beams through an innovative perturbative methodology', in Journal of Physics: Conference Series. IOP Publishing, p. 12060. https://doi.org/10.1088/1742-6596/2820/1/012060

Esen, İ., Koç, M. A. and Eroğlu, M. (2024) 'Effect of functionally graded carbon nanotube reinforcement on the dynamic response of composite beams subjected to a moving charge', Journal of Vibration Engineering & Technologies, 12(3), pp. 5203–5218. https://doi.org/10.1007/s42417-023-01192-0

Griebel, M. and Hamaekers, J. (2004) 'Molecular dynamics simulations of the elastic moduli of polymer–carbon nanotube composites', Computer methods in applied mechanics and engineering, 193(17–20), pp. 1773–1788. https://doi.org/10.1016/j.cma.2003.12.025

Han, Y. and Elliott, J. (2007) 'Molecular dynamics simulations of the elastic properties of polymer/carbon nanotube composites', Computational materials science, 39(2), pp. 315–323. https://doi.org/10.1016/j.commatsci.2006.06.011

Jasim, Z. M. and Abdulsamad, H. J. (2025) 'Investigation Of Free Vibration Behavior For Composite Sandwich Beams With A Composite Honeycomb Core.', Kufa Journal of Engineering, 16(1). https://doi.org/10.30572/2018/KJE/160111

Ke, L.-L., Yang, J. and Kitipornchai, S. (2010) 'Nonlinear free vibration of functionally graded carbon nanotube-reinforced composite beams', Composite Structures, 92(3), pp. 676–683.https://doi.org/10.1016/j.compstruct.2017.10.052

Khaleel, H.H., Al-Hadrayi, Z.M.R. (2025). Free vibration analysis of rotating functionally graded material beams on elastic foundations using the Homotopy Perturbation Method. Mathematical Modelling of Engineering Problems, Vol. 12, No. 8, pp. 2771-2780. https://doi.org/10.18280/mmep.120818

Khosravi, S., Arvin, H. and Kiani, Y. (2019) 'Vibration analysis of rotating composite beams reinforced with carbon nanotubes in thermal environment', International Journal of Mechanical Sciences, 164, p. 105187. https://doi.org/10.1016/j.ijmecsci.2019.105187

Kumar, Y. (2018) 'The Rayleigh–Ritz method for linear dynamic, static and buckling behavior of beams, shells and plates: A literature review', Journal of Vibration and Control, 24(7), pp. 1205–1227. https://doi.org/10.1177/1077546317694724

Li, H. et al. (2019) 'Application of first-order shear deformation theory for the vibration analysis of functionally graded doubly-curved shells of revolution', Composite Structures, 212, pp. 22–42. https://doi.org/10.1016/j.compstruct.2019.01.012

Li, L., Tang, H. and Hu, Y. (2018) 'Size-dependent nonlinear vibration of beam-type porous materials with an initial geometrical curvature', Composite Structures, 184, pp. 1177–1188. https://doi.org/10.1016/j.compstruct.2017.10.052

Liu, H., Lv, Z. and Wu, H. (2019) 'Nonlinear free vibration of geometrically imperfect functionally graded sandwich nanobeams based on nonlocal strain gradient theory', Composite Structures, 214, pp. 47–61. https://doi.org/10.1016/j.compstruct.2019.01.090

Liu, H., Wu, H. and Lyu, Z. (2020) 'Nonlinear resonance of FG multilayer beam-type nanocomposites: effects of graphene nanoplatelet-reinforcement and geometric imperfection', Aerospace Science and Technology, 98, p. 105702. https://doi.org/10.1016/j.ast.2020.105702

Mohamed, S. A. et al. (2022) 'A comparison of FEM and DIQM in investigating the nonlinear free vibration of axially functionally graded tapered microbeams with general boundary conditions', Composite Structures, 282, p. 115027. https://doi.org/10.1016/j.compstruct.2021.115027

Mohammed Rahi , Z. and H. Khaleel , H. (2025) "Modeling and Evaluation of Vibrational Behavior in Functionally Graded Ceramic-Metal Composite Beams", Kufa Journal of Engineering, 16(2), pp. 35–57. doi:10.30572/2018/KJE/160203.

Pang, F., Li, H., Du, Y., et al. (2018) 'Free vibration of functionally graded carbon nanotube reinforced composite annular sector plate with general boundary supports', Curved and Layered Structures, 5(1), pp. 49–67. https://doi.org/10.1515/cls-2018-0005

Pang, F., Li, H., Jing, F., et al. (2018) 'Application of first-order shear deformation theory on vibration analysis of stepped functionally graded paraboloidal shell with general edge constraints', Materials, 12(1), p. 69. https://doi.org/10.3390/ma12010069

Ranjbar, M. and Feli, S. (2019) 'Temperature-dependent analysis of axially functionally graded CNT reinforced micro-cantilever beams subjected to low velocity impact', Mechanics of Advanced Materials and Structures, 26(13), pp. 1154–1168. https://doi.org/10.1080/15376494.2018.1432788

Reddy, J. (2007) 'Nonlocal theories for bending, buckling and vibration of beams', International journal of engineering science, 45(2–8), pp. 288–307. https://doi.org/10.1016/j.ijengsci.2007.04.004

Roy, S., Petrova, R. S. and Mitra, S. (2018) 'Effect of carbon nanotube (CNT) functionalization in epoxy-CNT composites', Nanotechnology reviews, 7(6), pp. 475–485. https://doi.org/10.1515/ntrev-2018-0068

Sadiq, S. E. et al. (2025) 'Free Vibration Analysis In Innovative 3d Printing Sandwich Panaels For Aircraft Structure.', Kufa Journal of Engineering, 16(1). https://doi.org/10.30572/2018/KJE/160116

Shen, H.-S. (2009) 'Nonlinear bending of functionally graded carbon nanotube-reinforced composite plates in thermal environments', Composite Structures, 91(1), pp. 9–19. https://doi.org/10.1016/j.compstruct.2009.04.026

Shenas, A. G., Malekzadeh, P. and Ziaee, S. (2017) 'Vibration analysis of pre-twisted functionally graded carbon nanotube reinforced composite beams in thermal environment', Composite Structures, 162, pp. 325–340. https://doi.org/10.1016/j.compstruct.2016.12.009

Shi, Z. et al. (2017) 'An exact solution for the free-vibration analysis of functionally graded carbon-nanotube-reinforced composite beams with arbitrary boundary conditions', Scientific reports, 7(1), p. 12909. https://doi.org/10.1038/s41598-017-12596-w

Soni, S. K. et al. (2022) 'Functionally graded carbon nanotubes reinforced composite structures: An extensive review', Composite Structures, 299, p. 116075. https://doi.org/10.1016/j.compstruct.2022.116075

Wang, C. Y. and Zhang, L. C. (2008) 'A critical assessment of the elastic properties and effective wall thickness of single-walled carbon nanotubes', Nanotechnology, 19(7), p. 75705. https://doi.org/10.1088/0957-4484/19/7/075705

Xing-Wei, W. U. et al. (2023) 'Study on the Longitudinal Excitation Force Characteristics of Elastic Propellers', Noise and Vibration Control, 43(1), p. 7.

Zhang, H. et al. (2020) ‘Analysis of functionally graded carbon nanotube-reinforced composite structures: a review’, Nanotechnology Reviews, 9(1), pp. 1408–1426. https://doi.org/10.1515/ntrev-2020-0110

Ziadoon Mohammed Rahi, A., Al-Khazraji, A. N. and Shandookh, A. A. (2022) ‘Mechanical properties investigation of composite FGM fabricated from Al/Zn’, Open Engineering, 12(1), pp. 789–798. https://doi.org/10.1515/eng-2022-0347

Ziadoon, M. R. A., Al-Khazraji, A. N. and Shandookh, A. A. (2023) ‘The effect of elevated temperature on the properties of Al/Zn functionally gradient materials composites’, AIP Conference Proceedings, 2779(1), p. 20006. https://do i.org/10.1063/5.0142251